JACS Au
AN OPEN ACCESS JOURNAL OF THE AMERICAN CHEMICAL SOCIETY



pubs.acs.org/jacsau
Article

# Unraveling the Role of Solvation and Ion Valency on Redox-Mediated Electrosorption through In Situ Neutron Reflectometry and Ab Initio Molecular Dynamics

Riccardo Candeago, Hanyu Wang, Manh-Thuong Nguyen, Mathieu Doucet, Vassiliki-Alexandra Glezakou, James F. Browning, and Xiao Su*

Cite This: JACS Au 2024, 4, 919−929
Read Online

ACCESS | Metrics & More | Article Recommendations | Supporting Information

**ABSTRACT:** Solvation and ion valency effects on selectivity of metal oxyanions at redox−polymer interfaces are explored through in situ spatial-temporally resolved neutron reflectometry combined with large scale ab initio molecular dynamics. The selectivity of $ReO_4^-$ vs $MoO_4^{2-}$ for two redox-metallopolymers, poly(vinyl ferrocene) (PVFc) and poly(3-ferrocenylpropyl methacrylamide) (PFPMAm) is evaluated. PVFc has a higher Re/Mo separation factor compared to PFPMAm at 0.6 V vs Ag/AgCl. In situ techniques show that both PVFc and PFPMAm swell in the presence of $ReO_4^-$ (having higher solvation with PFPMAm), but do not swell in contact with $MoO_4^{2-}$. Ab initio molecular simulations suggest that $MoO_4^{2-}$ maintains a well-defined double solvation shell compared to $ReO_4^-$. The more loosely solvated anion ($ReO_4^-$) is preferably adsorbed by the more hydrophobic redox polymer (PVFc), and electrostatic cross-linking driven by divalent anionic interactions could impair film swelling. Thus, the in-depth understanding of selectivity mechanisms can accelerate the design of ion-selective redox-mediated separation systems for transition metal recovery and recycling.

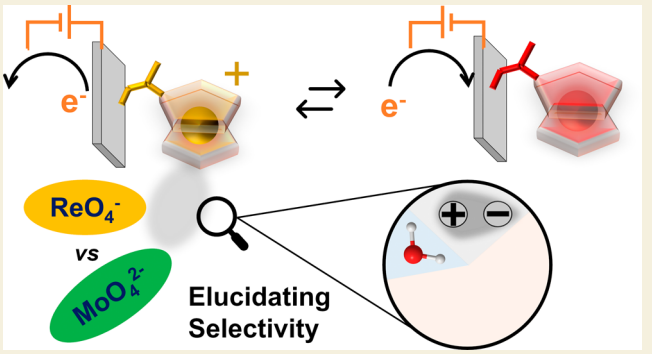


**KEYWORDS:** *electrochemical separations, neutron reflectometry, ab initio molecular dynamics, ion selectivity, electrosorption, redox-polymers, metallopolymers*

## 1. INTRODUCTION

Selective separation of metal ions from multicomponent mixtures represents a compelling challenge for critical materials recovery and recycling, as well as for environmental remediation.[1] Ion-electrosorption using redox metallopolymers features low energy consumption, no need for chemical regenerants, modularity, and scalability, making it an ideal candidate for both small and large scale separations; furthermore, adsorption and desorption of target anions is directly controlled by tuning the applied bias in a switch-like mechanism.[2−4] Currently, incomplete understanding of adsorption mechanisms taking place at redox-active interfaces constitutes a major bottleneck in rational design of better performing selective redox metallopolymers.[5] In particular, it is not clear how selectivity is influenced by solvation effects, ion valency, and morphological response of the film upon adsorption, at equilibrium and during the adsorption and desorption transients (i.e., in dynamic conditions).[3,6,7] In situ characterization of redox polymer behavior becomes a necessary step to advance separations, sensing, and energy technologies.[8] In this work, we provide a comprehensive study on the effects of solvation and ion valency on redox−polymer interface selectivity and behavior through in situ characterizations and ab initio molecular dynamics (AIMD) simulations.

Separation systems that target metals in their oxyanion form are essential for critical materials recovery and environmental remediation, because transition metals and main group elements are generally found as tetrahedral oxyanions in the environment and are extremely mobile in groundwaters.[9] Poly(vinyl ferrocene) (PVFc) is a prime example of a metallopolymer that can separate metal oxyanions with remarkable uptake (e.g., 103.1 mg-arsenic $g^{-1}_{adsorbent}$, 100 mg-chromium $g^{-1}_{adsorbent}$, and 120 mg-vanadate $g^{-1}_{PVFc}$) from aqueous and organic media in the presence of excess competing chloride or perchlorate, with low energy consumption.[2,10,11] Although PVFc has been extensively scrutinized using several in situ techniques,[3,12−18] only limited work has been devoted

Received: November 12, 2023
Revised: January 15, 2024
Accepted: January 17, 2024
Published: February 1, 2024

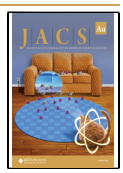

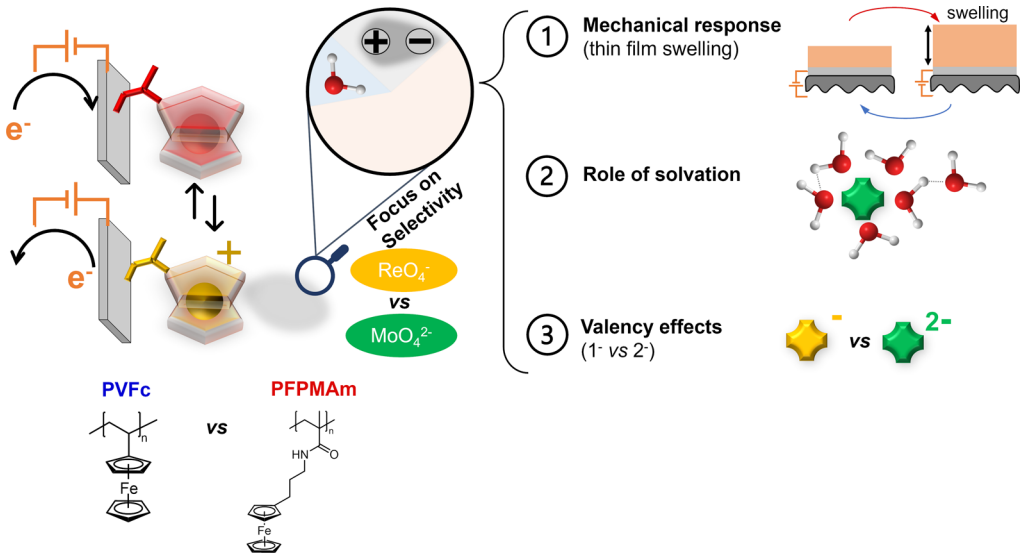


**Figure 1.** Schematics representing selective ion electrosorption through redox-active metallopolymer interfaces. Upon ferrocene oxidation, oxyanions are selectively adsorbed. The mechanisms driving selectivity were investigated through in situ measurements; namely, the morphological response of the film, the role of solvation, and valency effects were considered. PVFc and PFPMAm structures are represented.

to studying solvation effects.[12,15−19] Electrochemical quartz-crystal microbalance (EQCM) showed that different anions carry different amounts of solvent with them when ingressing PVFc films, and allowed to distinguish two ion ingression regimes: the permselective regime (at low salt concentrations), where only counterions and solvent penetrate the film, and the nonpermselective regime (above 1 M salt concentration), where ferrocene oxidation is coupled with both counterion and co-ion ingression.[17] EQCM measurements with anions of different sizes revealed two types of ferrocene sites: ∼58% of the sites occupy a compact, unsolvated environment that can undergo redox switching in $NaClO_4$ solutions with transfer of small counterions (such as $ClO_4^-$), while ∼42% of the sites are in a more solvated environment and initially undergo redox switching with the transfer of $ClO_4^-$ accompanied by ∼10−11 $H_2O$ molecules per adsorption site.[18] However, bulkier anions get progressively locked in the more solvated sites, diminishing the electroactivity of the film.[18] Successive studies tracked solvent ingression in thin PVFc films in contact with $NaClO_4$ through neutron reflectometry (NR) in both equilibrium and dynamic conditions, showing that PVFc films are comprised of three distinct sections in terms of solvation behavior: the inner polymer/electrode region (∼10% thickness), which showed greater than average solvation levels, the polymer/solution interfacial region (∼10% thickness), which registered a progressive transition to the pure solvent, and the bulk region; solvent volume fraction was estimated as ∼10% for the reduced state and ∼30% in the oxidized state for PVFc, with greater solvation in the center.[12,16] A previous experimental and computational approach analyzed binding and charge transfer interactions in ferrocene metallopolymer.[6] The analysis revealed that metal oxyanions with lower ionization energy are more sensitive to charge transfer effects upon binding with ferrocenium; furthermore, the separation factor is dependent on the applied potential in some binary competitive separations such as perrhenate vs molybdate and chromate vs molybdate.[6]

Nonetheless, an overall complete description of the mechanisms governing selective adsorption at redox−metallopolymer interfaces is still lacking; namely, there are no studies investigating the role that solvation and ion valency play in determining selectivity at redox-active metallopolymer interfaces. Understanding the role of solvation is crucial, since the extent of ion desolvation upon adsorption discriminates between specific and nonspecific adsorption at an electrochemical interface.[13,20]

In this study, we investigated how thin film morphological response, solvation, oxyanion valency, and dynamic effects influence the redox-active metallopolymer selectivity for metal oxyanions. We considered two redox-active metallopolymers with different hydrophilic/hydrophobic characters, namely, poly(vinyl ferrocene) (PVFc) and poly(3-ferrocenylpropyl methacrylamide) (PFPMAm) (Figure 1). We studied the separation of perrhenate ($ReO_4^-$) from molybdate ($MoO_4^{2-}$), a separation with high commercial and strategic relevance.[21,22] Rhenium is one of the rarest metals, having irreplaceable applications in high-temperature alloys and catalysis; it is extracted as a byproduct of molybdenum, copper, lead, and uranium mining.[21] Rhenium is found in aqueous solutions almost always as $ReO_4^-$.[22] Furthermore, $ReO_4^-$ is a common nonradioactive analogue for $TcO_4^-$.[23] $TcO_4^-$ is a major fission product in nuclear fuel wastes and is among the most hazardous radiation-derived contaminants due to the long half-life, high water solubility, and ability to migrate within the upper layer of the Earth's crust.[23] Rhenium is separated mainly through solvent extraction and ion exchange in the perrhenate form; solvent extraction, however, consumes significant amounts of acid or alkaline solutions in combination with organic extractants, which are toxic and environmentally hazardous.[21]

Neutron reflectometry allowed for the derivation of solvent fraction profiles under in situ conditions, revealing that PFPMAm is more solvated than PVFc, especially after a subsequent reduction step; also, information on film swelling/deswelling with subnanometer resolution was obtained, with both PVFc and PFPMAm swelling in the presence of $ReO_4^-$, but not of $MoO_4^{2-}$; spectroscopic ellipsometry (SE) was used as a complementary technique to measure film swelling/deswelling and facilitate NR data modeling, while EQCM allowed for coupling of gravimetric and coulometric


https://doi.org/10.1021/jacsau.3c00705
JACS Au 2024, 4, 919−929

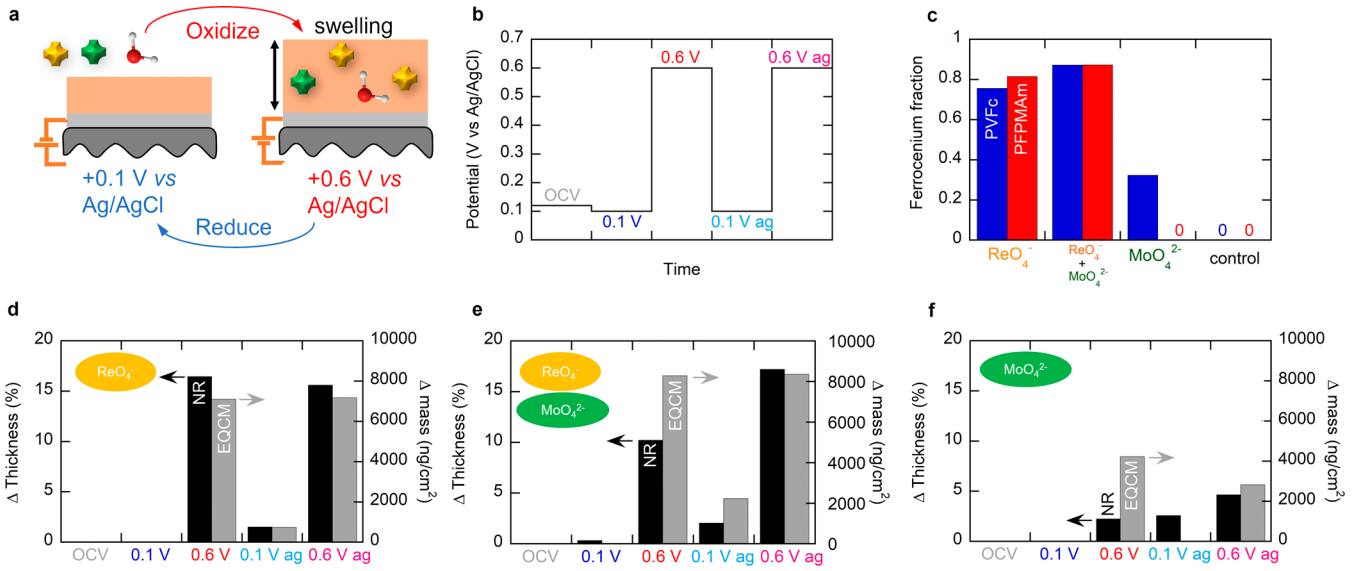


**Figure 2.** Morphological response of thin films. (a) Swelling/deswelling behavior of redox-active metallopolymers is dependent on the oxyanions in the bathing solution. (b) Schematics of the applied potential steps for thin-film experiments. (c) Fraction of ferrocenium estimated via X-ray photoelectron spectroscopy for PVFc and PFPMAm (5 min 0.1 V vs Ag/AgCl reduction followed by 15 min 0.6 V vs Ag/AgCl oxidation step, ex situ analysis). (d–f) Summary of in situ neutron reflectometry and quartz-crystal microbalance experiments on thin PVFc films. In the case of $ReO_4^-$ and the $ReO_4^-$ + $MoO_4^{2-}$ binary mixture, the polymer film swells/deswells with a corresponding mass increase/decrease upon oxidation/reduction; in the case of $MoO_4^{2-}$, however, limited thickness changes were observed.

information. Furthermore, AIMD simulations were used to corroborate experimental observations and obtain a greater mechanistic insight into the role of solvation and ion valency effects. We anticipate that a deeper understanding of the adsorption/desorption mechanisms at redox-active metallopolymer interfaces will unlock new pathways for the rational design of ion-electrosorption systems with a higher selectivity.

## 2. RESULTS AND DISCUSSION

### 2.1. Morphological Response of Thin Films

The swelling behavior of metallopolymer films under potential control was analyzed, and it was found that both PVFc and PFPMAm swell in the presence of $ReO_4^-$, but not of $MoO_4^{2-}$. X-ray photoelectron spectroscopy (XPS) showed lower ferrocene oxidation for PVFc and PFPMAm in the presence of $MoO_4^{2-}$ compared to $ReO_4^-$. Incomplete oxidation of the redox centers and/or valency effects leading to electrostatic cross-linking driven by divalent anionic interactions were evaluated to explain the different morphological responses of the thin films.

PVFc and PFPMAm thin films (~50 nm) were interrogated with in situ techniques under potential control: after an initial open circuit voltage (OCV) measurement, a sequence of reduction/oxidation steps (at 0.1 and 0.6 V vs Ag/AgCl, respectively, enough to respectively reduce or oxidize the film, as seen by the cyclic voltammetries in Figure S1) was applied to PVFc and PFPMAm thin films in aqueous single anion solutions and in an equimolar binary anion solution (20 mM $ReO_4^-$, 10 mM $ReO_4^-$ + 10 mM $MoO_4^{2-}$, 20 mM $MoO_4^{2-}$) (Figure 2a,b). Interface behavior was evaluated by using three distinct in situ techniques: NR, SE, and EQCM. Swelling was tracked with NR and SE, which yielded independent information on thickness changes, while net mass change at the interface was monitored through EQCM. For both PVFc and PFPMA, no swelling upon immersion of the films in anion-containing solutions was observed, with the OCV values indicating that the films were initially in the reduced state (~0.1 V vs Ag/AgCl). XPS confirmed that the as-cast metallopolymer films were in a reduced state (Figure 2c). No swelling nor mass uptake occurred upon the first application of a reducing potential (0.1 V vs Ag/AgCl). The first film oxidation (chronoamperometry at 0.6 V vs Ag/AgCl) led to different behaviors depending on the bathing solution: in the case of PVFc, the film swelled with a corresponding mass increase for both $ReO_4^-$ and $ReO_4^-$ + $MoO_4^{2-}$ (Figure 2d,e); however, even though little to no swelling was observed for $MoO_4^{2-}$, EQCM still recorded a mass increase (Figure 2f). Upon successive reduction (0.1 V vs Ag/AgCl), the films contracted with a corresponding net mass decrease for $ReO_4^-$ (mass decrease −89.5% for PVFc, −85.6% for PFPMAm) and for the binary $ReO_4^-$ + $MoO_4^{2-}$ mixture (mass decrease −73.1% for PVFc, −67.1% for PFPMAm). In the case of PVFc-$MoO_4^{2-}$, a mass decrease also took place upon reduction of the film. A successive oxidation step (at 0.6 V vs Ag/AgCl) showed that swelling and mass uptake were reversible (NR and SE details reported in Figures S5–S7). The behavior was similar for PFPMAm (Figures S8–S10). For PFPMAm-$MoO_4^{2-}$ experiments, the polymer interface was unstable upon oxidation, with the polymer partially or fully detaching from the electrode (Figures S10g,h and S13f). For both PVFc and PFPMAm in contact with the $ReO_4^-$ + $MoO_4^{2-}$ solution, film behavior was dominated by the $ReO_4^-$ character. We hypothesize that the dominating perrhenate-like character of the response could be linked to the higher selectivity of the interfaces toward perrhenate (see Section 2.2). We then investigated why neither solvent ingression nor film swelling took place for PVFc film in contact with just molybdate, possibly due to a lower degree of ferrocene oxidation and/or oxyanion valency effects, with electrostatic cross-linking impairing ingression of solvent and divalent anions (such as $MoO_4^{2-}$) in the film.


https://doi.org/10.1021/jacsau.3c00705
JACS Au 2024, 4, 919–929

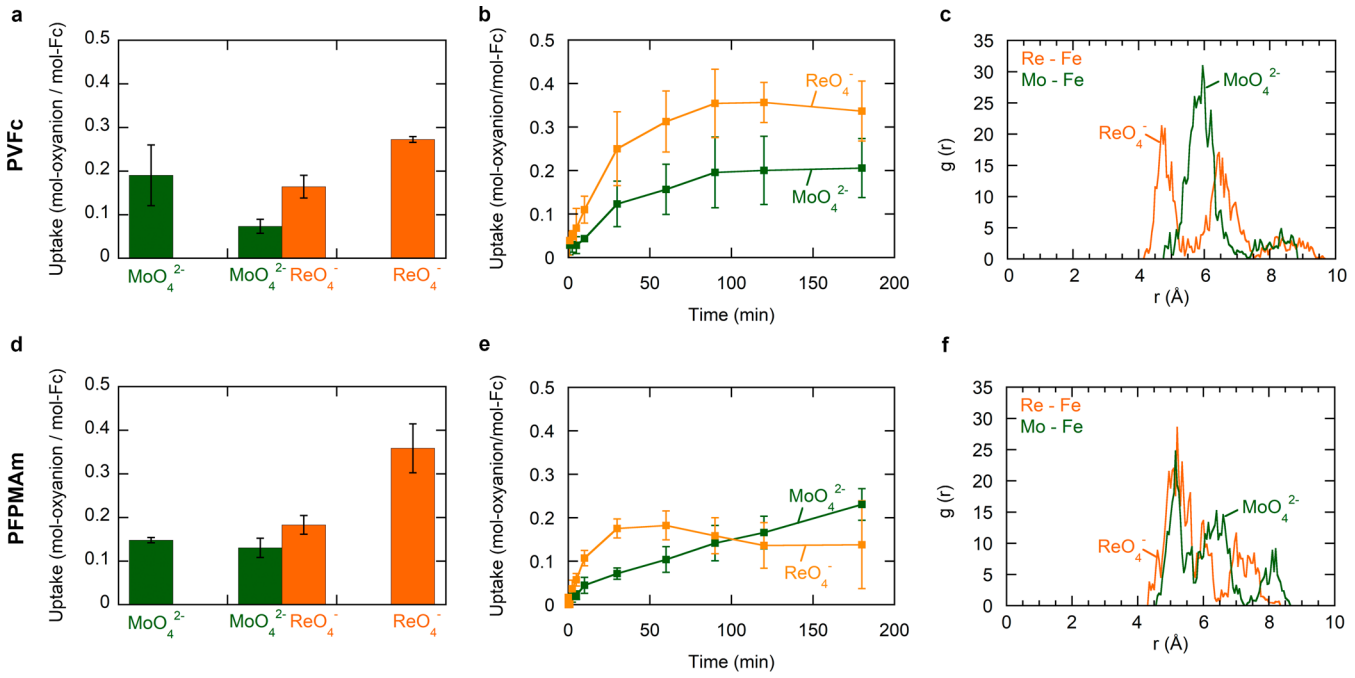


**Figure 3.** (a) Uptake of 1 mM $ReO_4^-$, 0.5 mM $ReO_4^-$ + 0.5 mM $MoO_4^{2-}$, 1 mM $MoO_4^{2-}$; 30 min adsorption for PVFc-CNT coated electrodes. Equilibrium $ReO_4^-$ vs $MoO_4^{2-}$ selectivity in the mixed oxyanion case was 3.1 for PVFc-CNT, and 1.5 for PFPMAm-CNT. (b) PVFc-CNT uptake kinetics at 0.6 V vs Ag/AgCl, equimolar binary mixture of $ReO_4^-$ and $MoO_4^{2-}$. (c) AIMD simulations showed selectivity for perrhenate over molybdate for PVFc. (d,e) 30 min uptake, uptake kinetics. (f) AIMD simulations showed no clear perrhenate-molybdate selectivity for PFPMAm.

Ex situ XPS analysis performed on thin films after an oxidation step at 0.6 V vs Ag/AgCl (Figure 2c) revealed that only 32% of ferrocene was oxidized to ferrocenium for the PVFc-$MoO_4^{2-}$ couple, whereas PVFc and PFPMAm in the presence of $ReO_4^-$ or in the binary $ReO_4^-$ + $MoO_4^{2-}$ mixture showed high ferrocenium fraction (76−87%). At a first glance, the lack of swelling and low uptake could be attributed to insufficient oxidation of ferrocene to ferrocenium, which would limit the number of available adsorption sites. However, the cumulative charge passed during the 0.6 V oxidative step is highest for molybdate as compared to perrhenate or the mixed oxyanion case for both PVFc and PFPMAm (Figure S13c,d), and the applied potential is not high enough to consider the oxygen evolution reaction as a competing faradaic process. Also, PFPMAm in contact with molybdate sometimes resulted in the film partially peeling off; EQCM measurements showed a linear loss of mass over charge behavior (Figure S13f), and XPS highlighted that the ferrocene redox centers remaining on the surface were completely reduced (Figure 2c). Thus, we hypothesize that the PFPMAm layer in contact with the electrolyte gradually binds to molybdate, leading to a partial delamination of the PFPMAm film upon oxidation. In the case of PVFc, there was a negligible mass change upon oxidation, which could be the result of the counteracting effects of adsorption on the surface and polymer peeling off and diffusing in the electrolyte. It was reported that bulky anions get locked in the polymer upon ferrocene oxidation;[18] however, the ionic radii of $ReO_4^-$ and $MoO_4^{2-}$ are 260 and 254 pm, respectively, suggesting that size of the ion is not responsible for the observed difference in swelling behavior.[24]

An electrostatically cross-linked gel could form upon oxidation of PVFc and PFPMAm if the divalent oxyanion $MoO_4^{2-}$ simultaneously interacts with two ferrocenium units. As a result, the ability of the film to swell/deswell would be impaired. It is also possible that once the metallopolymer gel forms, it can detach from the underlying reduced polymer. Physical cross-linking behavior would be in agreement with previous studies of polyelectrolyte systems in contact with divalent anions, where polyvalent ions enhance formation of cross-links between chains and a compact structure for the electrolyzed film.[25] AIMD simulations indicate that $MoO_4^{2-}$ interacts more strongly with PFPMAm than with PVFc, since the maximum of the first peak of Fe−Mo radials distribution function is located at ∼5.2 Å in the PFPMAm-$MoO_4^{2-}$ system and at ∼5.9 Å in the PVFc-$MoO_4^{2-}$ system, as shown in Figure 3c,f.

## 2.2. Selectivity of $ReO_4^-$ vs $MoO_4^{2-}$

In order to quantify anion uptake, separation experiments were run with larger electrodes (∼2−4 $cm^2$) made by coating carbon paper current collectors with redox polymer-carbon nanotube (CNT) ink. CNTs form a uniform noncovalent dispersion with PVFc and boost interface surface area.[26] These bulk experiments showed that $ReO_4^-$ was preferred over $MoO_4^{2-}$ by both PFPMAm-CNT and PVFc-CNT, but PVFc-CNT had a higher Re/Mo separation factor compared to that of PFPMAm-CNT, while adsorption kinetics revealed time-dependent selectivity. These findings are in agreement with AIMD simulations, which highlighted how in the case of PVFc the ferrocenium units interact more strongly with $ReO_4^-$ than with $MoO_4^{2-}$ while in the case of PFPMAm, the corresponding interactions are similar, as revealed by the radial distribution functions, $g(r)$, of Fe−Re and Fe−Mo atom pairs (Figure 3c,f).

Bulk binary adsorption kinetic experiments (at 0.6 V vs Ag/AgCl) showed that PFPMAm-CNT features a peak in separation factor at 15−30 min ($\alpha_{ReO_4^-,MoO_4^{2-}} = 2.9$), with the selectivity decreasing afterward; overall, PVFc-CNT displayed a stable $ReO_4^-$ vs $MoO_4^{2-}$ separation factor ($\alpha_{ReO_4^-,MoO_4^{2-}} = 2.3 - 2.7$) as a function of time (Figures 3b,e


https://doi.org/10.1021/jacsau.3c00705
JACS Au 2024, 4, 919−929

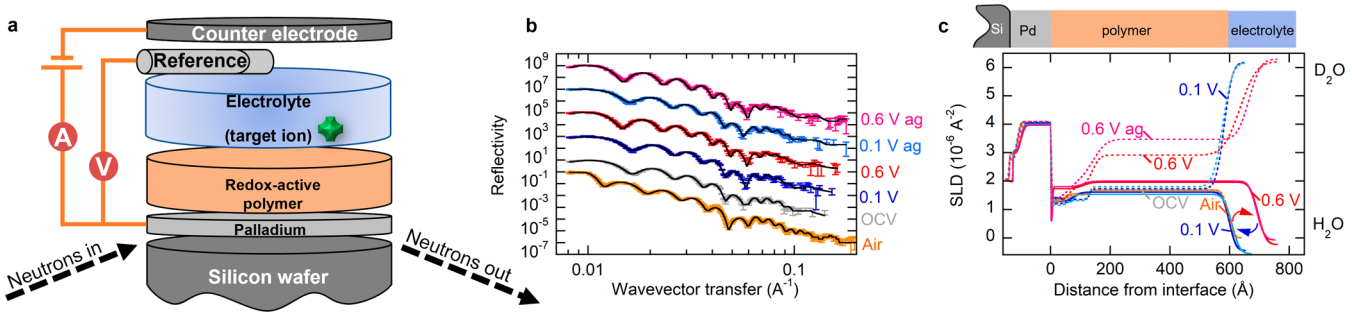


**Figure 4.** (a) Neutron reflectometry cell setup. (b) Example of reflectivity over a wavevector transfer curve (PVFc, $ReO_4^-$, $H_2O$) at different applied potentials. (c) Fitted data yield scattering length density over distance from the interface profiles.

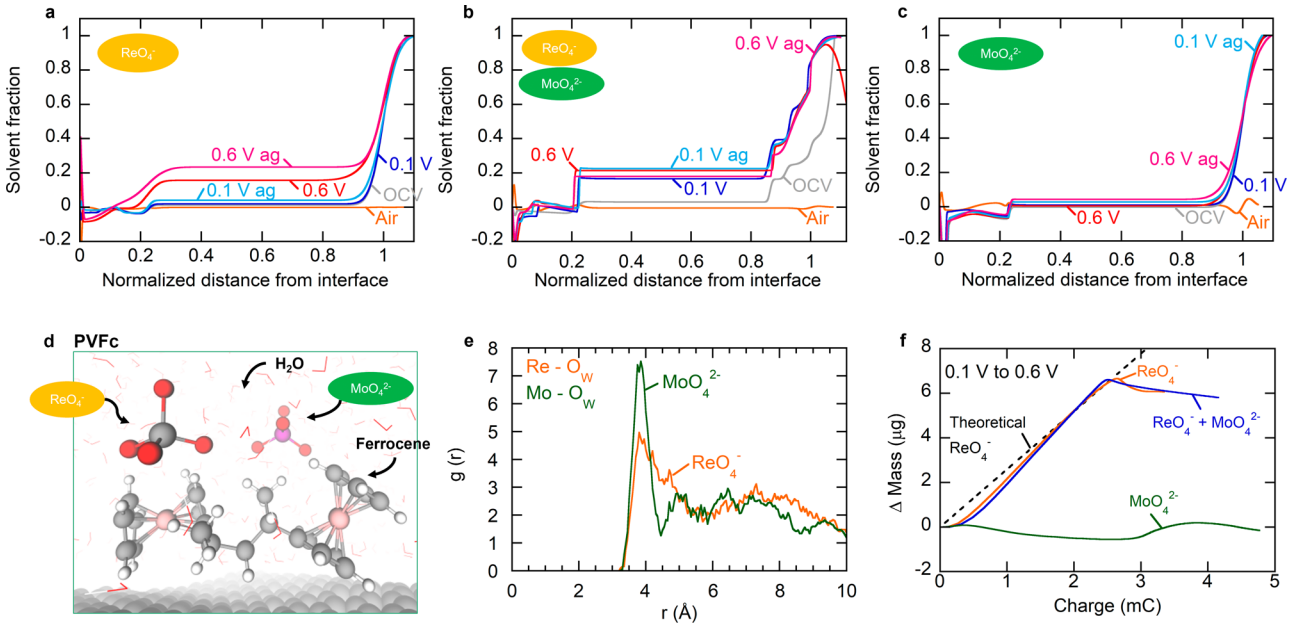


**Figure 5.** Solvation effects. (a–c) Solvation profiles obtained through neutron reflectometry; the movement of water can be isolated from salt and polymer through contrast variation with $H_2O$ and $D_2O$. (d) Snapshot of the AIMD simulation for PVFc. (e) AIMD showed that perrhenate is less solvated than molybdate in both the individual and binary solutions. (f) Mass and cumulative charge variation for the EQCM experiment at a chronoamperometric step (0.1–0.6 V vs Ag/AgCl) for a thin PVFc film, which allows us to estimate solvation numbers.

and S1g). Further bulk experiments run at 0.6 V vs Ag/AgCl for 30 min showed an equilibrium separation factor $\alpha_{ReO_4^-,MoO_4^{2-}} = 3.1$ for PVFc and 1.5 for PFPMAm (Figure 3a,d), as well as high oxyanion release upon application of a reducing potential (>72% desorption) except for PFPMAm-CNT in contact with $MoO_4^{2-}$ (47% release) (see Note S1, Figure S4). The selectivity in the case of PVFc-CNT was in line with previous results at the same applied potential ($\alpha_{ReO_4^-,MoO_4^{2-}} \sim 3.3$).[6] Selectivity for thin polymer films was estimated via XPS, yielding a Re/Mo separation factor of 2.1 for PVFc and 6.8 for PFPMAm (after 15 min at 0.6 V vs Ag/AgCl, Table S1).

## 2.3. Solvation Effects on Selectivity

We then addressed our main hypothesis that solvation plays a role in determining selectivity. We found that solvation does indeed play a major role, leading to higher selectivity for the less solvated oxyanion ($ReO_4^-$). Neutron reflectometry and EQCM allowed us to get complementary in situ information on the movement of water in the redox-polymer films.

In situ neutron reflectometry leverages the large scattering length density (SLD) difference between $H_2O$ (theoretical SLD $-0.56 \times 10^{-6}$ Å$^{-2}$) and $D_2O$ (theoretical SLD $6.4 \times 10^{-6}$ Å$^{-2}$) to isolate the movement and distribution of water—with subnanometer resolution—from the ion and polymer contributions to the SLD (Figure 4a). The specular reflection $R(Q)$ is measured at a glancing incident angle of $\theta$, and the measured intensity of the reflected neutron beam is usually expressed in terms of the wavevector transfer $Q$, with $Q = \frac{4\pi \sin\theta}{\lambda}$, where $\lambda$ is the neutron wavelength. The reflectivity profiles $R(Q)$ (Figure 4b) were modeled using a stack of layers, with each layer carrying information regarding the layer's thickness, SLD, as well as a measure of interfacial roughness (Figure S11); SLD depth profiles were thus obtained (Figure 4c). Solvent volume fraction as a function of film depth was also estimated for PVFc and PFPMAm in contact with 20 mM $ReO_4^-$, 20 mM $MoO_4^{2-}$, and an equimolar 10 mM binary mixture under a reducing (0.1 V vs Ag/AgCl) and oxidizing (0.6 V vs Ag/AgCl) potential, at equilibrium (for PVFc Figure 5a–c, for PFPMAm Figure S12). In the case of PVFc-$ReO_4^-$, redox-polymer oxidation was accompanied by solvent ingression (average solvent volume fraction of 0.8% in the initial reduced state vs 11.2% in the


https://doi.org/10.1021/jacsau.3c00705
JACS Au 2024, 4, 919–929

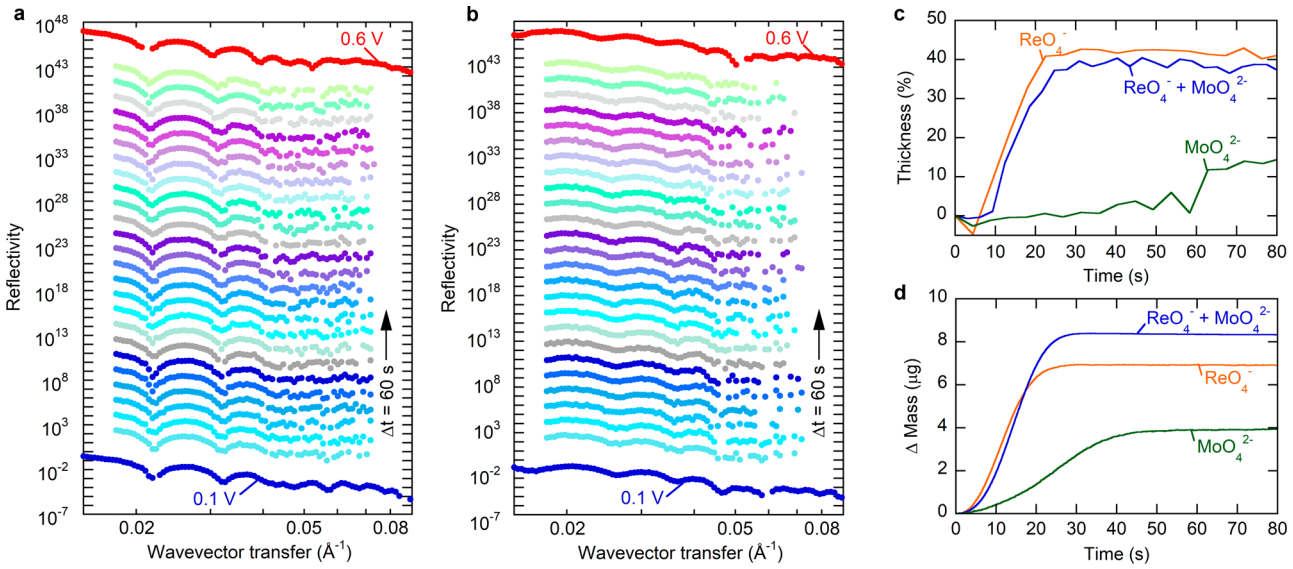


**Figure 6.** Dynamic data for PVFc. (a,b) In situ neutron reflectometry for 10 mM $ReO_4^-$ + 10 mM $MoO_4^{2-}$ solution in $D_2O$ and $H_2O$, respectively. Bottom and top curves are equilibrium runs, while the other curves are dynamic runs at 60 s intervals. (c) In situ spectroscopic ellipsometry for 20 mM $ReO_4^-$, 20 mM $MoO_4^{2-}$, and a mixed 10 mM $ReO_4^-$ + 10 mM $MoO_4^{2-}$ solution. (d) EQCM for 20 mM $ReO_4^-$, 20 mM $MoO_4^{2-}$, and mixed 10 mM $ReO_4^-$ + 10 mM $MoO_4^{2-}$ solution.

oxidized state); additionally, the solvent was almost completely expelled upon a successive reduction of the film (average solvent volume fraction of 2.6% upon successive reduction, Figure 5a). Solvent fraction for $ReO_4^-$ was lower than previously reported NR-estimated solvent fraction for $ClO_4^-$.[12,16] In the PFPMAm-$ReO_4^-$ case, upon oxidation, a larger amount of solvent entered in the film (average solvent volume fraction of 0.0% in the initial reduced state vs 17.3% in the oxidized state); also, upon reduction, a significant amount of solvent remained in the film (14.9%) (Figure S12). In contrast to this behavior, there was virtually no solvent for the PVFc-$MoO_4^{2-}$ couple in both the reduced and oxidized states, as PFPMAm peeled off when in contact with molybdate.

EQCM was used to determine solvation numbers by comparing the experimental slope of the mass over the cumulative charge curve with the theoretical slope calculated for oxyanions ingressing the film (Figure 5f). However, we could not distinguish between solvation of the anion and solvation of the ferrocenium unit, so we attributed the solvation numbers to the anion−ferrocenium pair. In fact, the contribution of ferrocenium to the solvation number was previously extrapolated as 4−5$H_2O$ per ferrocene site for PVFc by comparing gravimetric data of anions having different molecular masses.[17] The mass change was attributed entirely to counterion and solvent ingression, with no co-ion expulsion since our oxyanion concentrations (20 mM) corresponded to the permselective regime. In the case of PVFc, a solvation number of 2.2$H_2O$ per $ReO_4^-$-$Fc^+$ pair was estimated (experimental mass vs charge slope of 3.00 $\mu$g mC$^{-1}$) (Figure 5f). Nonetheless, in the case of $MoO_4^{2-}$, no net mass uptake was observed; therefore, the solvation number could not be estimated. The solvation of $ReO_4^-$ appeared to be quite low when we excluded the contribution of ferrocenium to solvation, suggesting that perrhenate was not very solvated when it was adsorbed to oxidized PVFc. In the case of $ReO_4^-$ in contact with PFPMAm, a solvation number of 3.9$H_2O$ per $ReO_4^-$-$Fc^+$ pair was estimated (experimental mass vs charge slope of 3.31 $\mu$g mC$^{-1}$), in line with the NR observation of a higher solvent fraction upon oxidation for PFPMAm. An experimental hydration number of 12$H_2O$/$MoO_4^{2-}$ in bulk water was previously reported.[24] Furthermore, the Gibbs energy of hydration is −1404 kJ/mol for $MoO_4^{2-}$ and −226 kJ/mol for $ReO_4^-$.[24] The increased solvation of the PFPMAm-$ReO_4^-$ couple suggests that the hydrogen bonding between the amide groups in PFPMAm and $H_2O$ could be responsible for the increased hydrophilicity of PFPMAm compared to PVFc.[27] The mass over charge behavior of the binary $ReO_4^-$−$MoO_4^{2-}$ mixture was similar to the one of just $ReO_4^-$, for both PVFc (Figure 5f) and PFPMAm (Figure S13f), with essentially the same mass over charge slopes; PFPMAm displayed overall higher solvent fraction throughout the film in the oxidized state, as well as higher solvation for ingressing $ReO_4^-$ anions. PFPMAm also retained more water in the first reduction after the oxidative step as compared to PVFc. Contact angle measurements highlighted PFPMAm being more hydrophilic than PVFc in its as-cast, reduced, and oxidized form, as shown by contact angle measurements (Figure S14). Our contact angle results are in agreement with changes in wettability upon oxidation previously reported for PVFc.[28]

AIMD simulations showed that upon adsorption, for both PVFc and PFPMAm systems, $MoO_4^{2-}$ interacts more strongly with water than $ReO_4^-$ does (for PVFc, see Figure 5d,e, and for PFPMAm, see Figure S16b). This is consistent with the previously reported behavior of these anions and their interactions with $H_2O$: $ReO_4^-$ is a "structure breaker", forming weaker and longer hydrogen bonds to water in its first hydration shell, whereas $MoO_4^{2-}$ is a "structure maker", meaning that it forms hydrogen bonds which are stronger than those in bulk water.[29] As a result, $ReO_4^-$ interacts more strongly with the polymer than $MoO_4^{2-}$ interacts with the polymer.

We found that solvation effects indeed play an important role; specifically, since perrhenate has a lower solvation energy and weaker hydrogen bonds in its first solvation shell, there is less of a barrier for $ReO_4^-$ to enter in the metallopolymer films compared to $MoO_4^{2-}$, which is bound with stronger hydrogen


https://doi.org/10.1021/jacsau.3c00705
JACS Au 2024, 4, 919−929

bonds to its first solvation shell and has higher solvation energy. We suggest that the more hydrophobic film facilitates the ingression of the least solvated anion. The binary mixture behavior observed with EQCM (Figure 5f) showed a clear perrhenate-like character, which can be explained by having just $ReO_4^-$ entering the film at very short times even in a binary mixture, possibly due to a smaller energy penalty associated with the loss of perrhenate's solvation shell. In the case of the more hydrophilic polymer PFPMAm, the progressive molybdate ingression leads to a decreasing Re/Mo separation factor over time (bulk adsorption kinetics, Figure S4g). The previously observed[6] potential-dependent selectivity for the perrhenate-molybdate binary separation could be tentatively explained by solvation effects: at lower applied potentials (0.5−0.6 V vs Ag/AgCl), the energy penalty for desolvation is too high for the more solvated anion, so that the less solvated ion is preferred; instead, at higher applied potentials (0.9−1.0 V vs Ag/AgCl), the desolvation energy is no longer a limiting factor, and other aspects such as charge transfer effects play a more predominant role in determining selectivity. Density functional theory calculations support our rationalization, since in the case of ferrocenium molybdate, binding energy is ∼10 kcal/mol, whereas for perrhenate, binding energy is ∼7.5 kcal/mol.[6] In essence, we suggest that at lower applied potentials, solvation effects dominate over charge transfer effects, although the latter become dominant at higher applied potentials, when desolvation energy is no longer a limiting factor. Another possible explanation points to dynamic effects, which could be responsible for the difference in potential-dependent selectivity, with the selectivity being a function of time. We propose that a combination of in situ spectroscopic ellipsometry and EQCM offers a facile way to screen multiple binary ion couples under dynamic conditions with high throughput.

### 2.4. Dynamic Behavior of the Redox Interface

Preliminary results indicate that in situ ellipsometry, EQCM, and NR are effective at tracking dynamic changes taking place at the interface (Figures 6 and S15). The kinetics for rhenium electrosorption can be seen to be clearly faster than those for molybdenum, which also reflect observations seen for the time-dependent selectivity in Figure 3. Furthermore, kinetics of the ion mixture also reflect the kinetics of rhenium, in accordance with the NR and previous observations confirming rhenium selectivity in PVFc. Future work will involve elucidating the dynamic character of the selectivity factor and taking a deeper look at the behavior of interfaces under dynamic conditions. Kinetically controlled redox-polymer responses might allow for access to a variety of metastable states,[18] possibly leading to kinetically based separations instead of equilibrium-based separations.

## 3. CONCLUSIONS

In summary, redox-active metallopolymer interfaces are a promising candidate for energetically and chemically efficient ion-electrosorption systems, allowing for control of target metal oxyanion capture/release by tuning the applied potential. In this work, we explored solvation and ion valency effects on metal oxyanion selectivity as well as the morphological response of thin films upon adsorption/desorption. We analyzed metallopolymer film swelling behavior under potential control finding that both PVFc and PFPMAm swell in the presence of $ReO_4^-$, but not of $MoO_4^{2-}$. XPS showed lower ferrocene oxidation for PVFc and PFPMAm in the presence of $MoO_4^{2-}$ compared to $ReO_4^-$. We suggest that $MoO_4^{2-}$, being a divalent anion, physically cross-links oxidized PVFc and PFPMAm, impairing film swelling. Bulk separations demonstrated that $ReO_4^-$ was preferred over $MoO_4^{2-}$ by both PFPMAm-CNT and PVFc-CNT, but PVFc-CNT had a higher Re/Mo separation factor compared to that of PFPMAm-CNT, while adsorption kinetics displayed time-dependent selectivity. AIMD showed a greater difference in the adsorption of $ReO_4^-$ and $MoO_4^{2-}$ in the case of PVFc compared to PFPMAm. We determined that solvation has a significant effect on selectivity; namely, the less solvated oxyanion ($ReO_4^-$) was preferred over the more solvated oxyanion ($MoO_4^{2-}$), and higher separation factors were registered for the more hydrophobic polymer (PVFc). Our observations suggest that PFPMAm and PVFc prefer oxyanions with smaller solvation shells.

Hence, we propose that increased polymer hydrophobicity can improve separation factors, with a preference for the less solvated oxyanion. Modulating the film hydrophilic/hydrophobic character of metallopolymers appears as a viable way to tune the selectivity of the ion-electrosorption system. Future work will explore dynamic effects at the interface, time- and potential-dependent selectivity, and the characterization of separation factors for more hydrophobic polymers.

## 4. EXPERIMENTAL SECTION/METHODS

### 4.1. Bulk Separation

PFPMAm was synthesized through free radical polymerization as previously described [gel permeation chromatography (GPC) in THF using polystyrene calibration yielding $M_n$ = 25.4 kg mol$^{-1}$, $M_w$ = 144.5 kg mol$^{-1}$, $Đ$ = 5.6].[30] PVFc (16 mg, Polysciences, GPC-MALLS: absolute molecular weight $M_n$ = 1.5 kg mol$^{-1}$, $M_w$ = 3.2 kg mol$^{-1}$, $Đ$ = 2.2),[31] multiwalled carbon nanotubes (16 mg, as-produced cathode deposit, >7.5% MWCNT basis, O.D. × L 7−15 nm × 0.5−10 $\mu$m, Sigma-Aldrich), and chloroform (4 mL, >99.8%, Fisher Scientific) were sonicated in icy water (1 h) to form a PVFc-CNT ink. Carbon nanotubes were used so to enhance conductivity and surface area of the interface.[11] The same procedure was followed with PFPMAm (16 mg) to give PFPMAm-CNT ink. ∼50 $\mu$L of the ink was drop-cast on carbon paper over a 1 cm × 1 cm surface (Toray carbon paper, 5% wet-proofed with Teflon, FuelCellStore). The net mass of PVFc-CNT or PFPMAm-CNT was determined by weighing the carbon paper before and after coating with the ink, after complete evaporation of the solvent. One mM $NaReO_4$ (99.95%, Alfa Aesar), 1 mM $Na_2MoO_4$ (>98%, Sigma-Aldrich), and 0.5 mM $NaReO_4$ + 0.5 mM $Na_2MoO_4$ were prepared in DI-water (18.2 MΩ, Purelab Elga, UK). Electrosorption experiments were conducted at chronoamperometric conditions for 30 min using 1 mL of solution with a potentiostat (Squidstat Prime, Admiral Instruments) in a three-electrode configuration: Ag/AgCl (3.4 M KCl) leakless reference electrode (eDAQ), platinum wire counter electrode, and working electrode consisting of PVFc-CNT or PFPMAm-CNT (∼0.5 mg) on carbon paper. PFPMAm used for adsorption kinetics experiments was synthesized through free radical polymerization as previously described[30] (GPC in DMF with 1 g L$^{-1}$ LiBr using polystyrene calibration $M_n$ = 19.7 kg mol$^{-1}$, $M_w$ = 44.4 kg mol$^{-1}$, $Đ$ = 2.25, Figure S17a). Chromatograms are reported in Figure S17. PVFc synthesized for adsorption kinetics experiments was also synthesized through free radical polymerization as described elsewhere[32] (GPC in DMF with LiBr using polystyrene calibration $M_n$ = 2.5 kg mol$^{-1}$, $M_w$ = 4.0 kg mol$^{-1}$, $Đ$ = 1.6, Figure S17b). In the case of adsorption kinetics, larger electrodes were used (∼4 cm$^2$ coated area and 2.5−3.5 mg of polymer-CNT coating) with a correspondingly larger solution volume (20 mL). At least three replicates were run for each adsorption/desorption experiment. Both for adsorption kinetics (3 h) and adsorption experiments (30 min), 50 $\mu$L aliquots of solution were


https://doi.org/10.1021/jacsau.3c00705
JACS Au 2024, 4, 919−929

diluted (1:200) in 2% $HNO_3$ (certified ACS plus, Fischer Scientific) and used to measure Re and Mo concentrations through ICP-OES (5110 ICP-OES, Agilent Technologies). A 9 h adsorption kinetics (two replicates) using the same PFPMAm batch used for in situ experiments is reported in Figure S19. The wavelengths 197.248 nm (for Re) and 202.032 nm (for Mo) were used to calculate concentration values; no interference between Mo and Re lines was observed. Calibration curves were prepared in house from 1000 ppm Re and Mo standards (Sigma-Aldrich). Uptake was calculated as $\frac{(c_{M,stock} - c_{M,ads})V}{m_{adsorbent}} \frac{MW_{MO4}}{MW_M}$, where $c_{M,stock}$ is the initial metal stock concentration (M = Re, Mo), $c_{M,ads}$ is the metal concentration in solution after adsorption, $m_{adsorbent}$ is the mass of adsorbent material (including both polymer and carbon nanotubes), and $MW_{MO4}$ and $MW_M$ are the molecular weights of the oxyanion and of the metal, respectively. When uptake was expressed in molar terms, it was assumed that the polymer represented 50% of the adsorbent mass. Desorption took place in 20 mM NaCl (Sigma-Aldrich) and was calculated as $\frac{c_{M,des}}{c_{M,stock} - c_{M,ads}}$, where $c_{M,des}$ is the metal concentration in solution after desorption, with the adsorption and desorption volumes being equal.

### 4.2. EQCM

EQCM with dissipation monitoring (BluQCM QSD and SP-200 potentiostat, BioLogic) was used with 5 MHz, 14 mm Au/Cr or Au/Ti sensors (QuartzPro). Sensors were used as received. Previous reports showed that gold/PVFc adhesion is rather strong.[12] Experiments were run at constant temperature (23.0 °C), with 4−5 mL of 20 mM $NaReO_4$, 20 mM $Na_2MoO_4$, and 10 mM $NaReO_4$ + 10 mM $Na_2MoO_4$. The theoretical slope of mass vs charge curves was estimated as $\frac{MW_{anion}}{nF}$, where $MW_{anion}$ is the molecular weight of the anion, $n$ is the valency of the anion, and $F$ is Faraday's constant. 100% Faradaic efficiency is assumed, i.e., all the charge passed just oxidizes ferrocene to ferrocenium, without side reactions. Solvation numbers were estimated as $\frac{\text{experimental slope} - \frac{MW_{anion}}{nF}}{\frac{MW_{H_2O}}{F}}$, where $MW_{anion}$ is the molecular weight of water. In the case of EQCM measurements followed by XPS, the following potential steps were used: 5 min at 0.1 V vs Ag/AgCl followed by 15 min at 0.6 V vs Ag/AgCl; samples were not rinsed before XPS analysis, and the films were kept in the dark until XPS analysis. Multiple overtones were measured (up to the 13th overtone), and the change in frequency divided by the overtone number ($\Delta f/n$) did not show significant deviations for all overtones, thus the Sauerbrey equation was applied to estimate mass changes based on frequency changes.[33] The EQCM sensitivity of the sensors was −17.524 ng $Hz^{-1}$; this sensitivity was experimentally measured through EQCM calibration (see Note S2 and Figure S18).

### 4.3. Spectroscopic Ellipsometry

Thin film thickness was measured via ellipsometry (J.A. Woollam Variable-Angle Spectroscopic Ellipsometer). Spectroscopic scans (300−1000 nm wavelength range) were run at three angles of incidence (65, 70, and 75°). Measurements were performed at room temperature. Ellipsometric data were fitted with V.A.SE software (Note S3). In situ ellipsometry was carried out using an ellipsometry electrochemical cell with a 70° angle of incidence (redox.me, Sweden) and with a potentiostat (Squidstat Solo, Admiral Instruments). Figures S7 and S10 report both the measured data and the fitted model of the spectroscopic scans (Ψ and Δ vs wavelength) for the in situ ellipsometry measurements.

### 4.4. Neutron Reflectometry

Silicon wafers (2 in. diameter, 5 mm thickness, El-Cat, USA and ITME, Poland) were first cleaned in a clean room with DI-water, followed by acetone and isopropyl alcohol. The silicon wafers were then coated with palladium (∼10 nm thick coating, monitored by the in-house EQCM sensor, later confirmed by ellipsometry) via magnetron sputtering (base pressure <4 × $10^{-6}$ Torr, AJA ORION 3 with ST20 ORION magnetron sputter guns); the gas used was argon with a process pressure of 3.9 mTorr, DC power of 12 W, 60 s ramp, resulting in a sputtering rate of 1.1 Å/s. Silicon wafers were then quickly rinsed with isopropyl alcohol and dried with nitrogen. 7.5 mg/mL PVFc (Polysciences) and PFPMAm solutions in chloroform (>99.8%, Fisher Scientific) were filtered (Teflon syringe filter, 0.20 μm) so to improve the film quality, similarly to Glidle et al.[12] Spin coating was performed in a clean room at 2000 rpm for 60 s, with an acceleration of 1000 rpm $s^{-1}$, and ∼0.5 mL of the polymer solution was used.

Measurements were performed at Oak Ridge National Laboratory's Spallation Neutron Source using the Liquids Reflectometer (beamline BL-4B) and a potentiostat (VSP, BioLogic). Dry sample thickness was first measured for all samples. 20 mM $NaReO_4$ (99.95%, Alfa Aesar), $Na_2MoO_4$ single anion solutions in $H_2O$ and $D_2O$ (99.9 atom % D, Cambridge Isotope Laboratories, Inc.), and a 10 mM $ReO_4^-$ + 10 mM $MoO_4^{2-}$ binary solution were used (∼3 mL per run). The electrochemical setup included a TiZr counter electrode, PFPMAm/Pd/Si or PVFc/Pd/Si working electrode, and a Ag/AgCl reference electrode (Figure 4a reports the setup schematics). Equilibrium data were collected with a 1.7 × $10^{-2}$ to 5 × $10^{-2}$ $Å^{-1}$ wavevector transfer window. Dynamic data were collected with a 8 × $10^{-3}$ to 2 × $10^{-1}$ $Å^{-1}$ wavevector transfer window; the continuously acquired data points were then grouped into 15 s slices. Several models were tested with and without a hydration layer to ascertain that each layer was necessary to obtain a good fit. The NR data was modeled using the DREAM[34] fitting engine implemented within the refl1d[35] package. This fitting engine uses a Markov Chain Monte Carlo algorithm to sample the posterior probability in the parameter space of the model for optimization and uncertainty estimation. Details on calculation of solvent fraction from SLD profiles are discussed in Note S4.

### 4.5. X-ray Photoelectron Spectroscopy

Source gun type Al K$\alpha$, 400 μm spot size, CAE pass energy of 150.0 eV for survey or 50.0 eV for high resolution scans, and energy step size of 1.00 eV for surveys or 0.1 eV for high resolution scans. Shirley background was used for Fe 2p, Mo 3d, and Re 4f. All spectra were calibrated with the C 1s peak at 284.8 eV. For Fe 2p fitting, the approach by Su et al. was followed.[36] Lorentzian−Gaussian line shapes were used, and the area of the Fe $2p_{1/2}$ component was constrained as half of the Fe $2p_{3/2}$ area. The fraction of ferrocenium was estimated as $\frac{\text{area Fe } 2p_{3/2} \text{ oxidized}}{\text{area Fe } 2p_{3/2} \text{ oxidized} + \text{area Fe } 2p_{3/2}}$. Data were analyzed using CasaXPS (UIUC license), and the raw data are reported in Figures S2 and S3.

### 4.6. Contact Angle

Pendant drop measurements (Ramé-Hart model 250 Standard Goniometer) were conducted using deionized water (4−5 μL droplets) on as-cast, reduced (15 min at 0 V vs Ag/AgCl, 0.1 M $NaClO_4$), and oxidized (15 min at 0.6 V vs Ag/AgCl, 0.1 M $NaClO_4$) PVFc and PFPMAm thin films. Images were processed with DROPimage Advanced software.

### 4.7. Ab Initio Molecular Dynamics

To simulate the adsorption of cations on ferrocene polymers, we adopted truncated models of two PVFc/PFPMAm monomers supported on a graphene surface (1.71 × 1.48 $nm^2$). These systems are interfaced with 170 water molecules. Each system also contains 2 anions: 2 $ReO_4^-$, or 2 $MoO_4^{2-}$, or 1 $ReO_4^-$ and 1 $MoO_4^{2-}$. 1 or 2 $Na^+$ counterions were added to the systems to balance the charge of the anions (subject to the charge of the ferrocenium ion). Totally, the simulation cells consist of approximately 610/700 atoms for the systems with PVFc/PVFMAm.

We carried out ab initio molecular dynamics (AIMD) simulation using the CP2K program.[37] The PBE-D3 density functional[38] was adopted. We used the hybrid Gaussian-Plane wave basis set scheme,[39] in which the double-$\zeta$ Gaussian basis sets[40] were used to expand Kohn−Sham orbitals and a plane-wave cutoff of 450 Ry was used to compute electrostatic terms. The GTH pseudopotentials[41] were employed to describe the core electrons. In self-consistent calculations, only the Γ-point was considered and the surface dipole


https://doi.org/10.1021/jacsau.3c00705
JACS Au 2024, 4, 919−929

correction[42] for asymmetric slabs was applied. The low spin state of ferrocenium was found, consistent with the literature.[43]

Molecular dynamics simulations were carried out within the canonical (*NVT*) ensemble where the temperature was maintained by the Nose−Hoover thermostat.[44] This temperature, being higher than RT, helps accelerate the dynamics in the systems due to the limited AIMD time scale. A time step of 1 fs was used.

Water, anions, and $Na^+$ counterions were added to the polymer/graphene systems at random. As preparation for equilibrated systems, after static optimizations to local minima, 10 ps AIMD runs at a relatively high $T$ = 373 K were performed, moving the systems to low energy structures. This was followed by an annealing procedure to reduce the temperature to 333 K and 5 ps simulations at this temperature to further equilibrate the systems. Statistics reported in this work was obtained from 10 ps production runs.

## ■ ASSOCIATED CONTENT

### Supporting Information

The Supporting Information is available free of charge at https://pubs.acs.org/doi/10.1021/jacsau.3c00705.

Experimental details, gel permeation chromatography, EQCM calibration, ellipsometry modeling, adsorption kinetics, cyclic voltammetries, neutron reflectometry and spectroscopic ellipsometry raw data and depth profiles, solvent volume fraction for PFPMAm, EQCM characterization, XPS spectra, contact angle measurements, and ab initio molecular dynamics (PDF)

## ■ AUTHOR INFORMATION


### Corresponding Author

**Xiao Su** − *Department of Chemical and Biomolecular Engineering, University of Illinois at Urbana—Champaign, Urbana, Illinois 61801, United States;* orcid.org/0000-0001-7794-290X; Email: x2su@illinois.edu

### Authors

**Riccardo Candeago** − *Department of Chemical and Biomolecular Engineering, University of Illinois at Urbana—Champaign, Urbana, Illinois 61801, United States*

**Hanyu Wang** − *Center for Nanophase Materials Sciences, Oak Ridge National Laboratory, Oak Ridge, Tennessee 37831, United States;* orcid.org/0000-0001-8703-0293

**Manh-Thuong Nguyen** − *Physical and Computational Sciences Directorate, Pacific Northwest National Laboratory, Richland, Washington 99354, United States;* orcid.org/0000-0003-1997-0368

**Mathieu Doucet** − *Neutron Scattering Division, Oak Ridge National Laboratory, Oak Ridge, Tennessee 37831, United States;* orcid.org/0000-0002-5560-6478

**Vassiliki-Alexandra Glezakou** − *Oak Ridge National Laboratory, Oak Ridge, Tennessee 37831, United States;* orcid.org/0000-0001-6028-7021

**James F. Browning** − *Neutron Scattering Division, Oak Ridge National Laboratory, Oak Ridge, Tennessee 37831, United States;* orcid.org/0000-0001-8379-259X

Complete contact information is available at: https://pubs.acs.org/10.1021/jacsau.3c00705


### Author Contributions

CRediT: **Riccardo Candeago** conceptualization, data curation, formal analysis, investigation, methodology, validation, visualization, writing-original draft, writing-review & editing; **Hanyu Wang** data curation, formal analysis, investigation, methodology, project administration, resources, software, validation, visualization, writing-original draft, writing-review & editing; **Manh-Thuong Nguyen** data curation, formal analysis, investigation, methodology, resources, software, validation, visualization, writing-original draft, writing-review & editing; **Mathieu Doucet** data curation, formal analysis, investigation, methodology, software, validation, visualization, writing-original draft, writing-review & editing; **Vassiliki-Alexandra Glezakou** formal analysis, investigation, methodology, resources, software, supervision, validation, visualization, writing-review & editing; **James F. Browning** formal analysis, investigation, methodology, project administration, resources, supervision, writing-review & editing; **Xiao Su** conceptualization, funding acquisition, investigation, methodology, project administration, supervision, writing-original draft, writing-review & editing.

### Notes

The authors declare no competing financial interest.

## ■ ACKNOWLEDGMENTS

This material is based upon work supported by the U.S. Department of Energy, Office of Science, Office of Basic Energy Sciences Separations Science program, under Award Number DE-SC0021409 for X.S. M.-T.N was supported by the U.S. Department of Energy (DOE), Office of Science, Office of Basic Energy Sciences, Chemical Sciences, Geosciences, and Biosciences Division, project 81462 (Harnessing Confinement Effects, Stimuli, and Reactive Intermediates in Separations). V.-A.G. acknowledges support from the LDRD program at ORNL. We thank Johannes Elbert for the synthesis of PFPMAm and PVFc, Haley Vapnik for the DSC analysis, Jisoo Choi, Beichen Xiong, and Celine Sutio for running bulk separation experiments. We also thank Jose Luis Vazquez for the graphics design of our cover art, and Dr. Cara Touretzky for providing the artistic concept. Spectroscopic ellipsometry, contact angle measurements, magnetron sputtering, spin coating in clean room were carried out in the Illinois Materials Research Laboratory Central Research Facilities, University of Illinois. A portion of this research used resources at the Spallation Neutron Source (SNS), a Department of Energy (DOE) Office of Science User Facility operated by Oak Ridge National Laboratory. Neutron reflectometry measurements were carried out on the Liquids Reflectometer at the SNS, which is sponsored by the Scientific User Facilities Division, Office of Basic Energy Sciences, DOE.

## ■ REFERENCES

(1) Bauer, D. J. N.; Ruby, T.; Smith Braeton, J. *Critical Materials Assessment*; U.S. Department of Energy, 2023. (b) Hu, J.; Jiang, Y.; Li, L.; Yu, Z.; Wang, C.; Gill, G.; Xiao, J.; Cavagnaro, R. J.; Kuo, L.-J.; Asmussen, R. M.; et al. A Lithium Feedstock Pathway: Coupled Electrochemical Extraction and Direct Battery Materials Manufacturing. *ACS Energy Lett.* **2022**, *7* (8), 2420−2427.

(2) (a) Su, X.; Hatton, T. A. Redox-electrodes for selective electrochemical separations. *Adv. Colloid Interface Sci.* **2017**, *244*, 6−20. (b) Hübner, H.; Candeago, R.; Schmitt, D.; Schießer, A.; Xiong, B.; Gallei, M.; Su, X. Synthesis and covalent immobilization of redox-active metallopolymers for organic phase electrochemistry. *Polymer* **2022**, *244*, 124656.

(3) Su, X. Electrochemical interfaces for chemical and biomolecular separations. *Curr. Opin. Colloid Interface Sci.* **2020**, *46*, 77−93.

(4) (a) Kim, K.; Candeago, R.; Rim, G.; Raymond, D.; Park, A.-H. A.; Su, X. Electrochemical approaches for selective recovery of critical elements in hydrometallurgical processes of complex feedstocks.

*iScience* **2021**, *24* (5), 102374. (b) Kim, K.; Zagalskaya, A.; Ng, J. L.; Hong, J.; Alexandrov, V.; Pham, T. A.; Su, X. Coupling nitrate capture with ammonia production through bifunctional redox-electrodes. *Nat. Commun.* **2023**, *14* (1), 823. (c) Vapnik, H.; Elbert, J.; Su, X. Redox-copolymers for the recovery of rare earth elements by electrochemically regenerated ion-exchange. *J. Mater. Chem. A* **2021**, *9* (35), 20068−20077. (d) Candeago, R.; Kim, K.; Vapnik, H.; Cotty, S.; Aubin, M.; Berensmeier, S.; Kushima, A.; Su, X. Semiconducting Polymer Interfaces for Electrochemically Assisted Mercury Remediation. *ACS Appl. Mater. Interfaces* **2020**, *12* (44), 49713−49722.

(5) Kim, N.; Oh, W.; Knust, K. N.; Zazyki Galetto, F.; Su, X. Molecularly Selective Polymer Interfaces for Electrochemical Separations. *Langmuir* **2023**, *39* (47), 16685−16700.

(6) Chen, R.; Feng, J.; Jeon, J.; Sheehan, T.; Rüttiger, C.; Gallei, M.; Shukla, D.; Su, X. Structure and Potential-Dependent Selectivity in Redox-Metallopolymers: Electrochemically Mediated Multicomponent Metal Separations. *Adv. Funct. Mater.* **2021**, *31* (15), 2009307.

(7) Goyal, P.; Kusoglu, A.; Weber, A. Z. Coalescing Cation Selectivity Approaches in Ionomers. *ACS Energy Lett.* **2023**, *8* (3), 1551−1566.

(8) (a) Xu, J.; Koh, M.; Minteer, S. D.; Korzeniewski, C. In Situ Confocal Raman Microscopy of Redox Polymer Films on Bulk Electrode Supports. *ACS Meas. Sci. Au* **2023**, *3* (2), 127−133. (b) Keene, S. T.; Gueskine, V.; Berggren, M.; Malliaras, G. G.; Tybrandt, K.; Zozoulenko, I. Exploiting mixed conducting polymers in organic and bioelectronic devices. *Phys. Chem. Chem. Phys.* **2022**, *24* (32), 19144−19163. (c) Beebee, C.; Watkins, E. B.; Sapstead, R. M.; Ferreira, V. C.; Ryder, K. S.; Smith, E. L.; Hillman, A. R. Effect of electrochemical control function on the internal structure and composition of electrodeposited polypyrrole films: A neutron reflectometry study. *Electrochim. Acta* **2019**, *295*, 978−988. (d) Maibach, J.; Rizell, J.; Matic, A.; Mozhzhukhina, N. Toward Operando Characterization of Interphases in Batteries. *ACS Mater. Lett.* **2023**, *5* (9), 2431−2444.

(9) Smith, P.; Barr, M.; Barrans, R. *Separations Chemistry of Toxic Metals*; Los Alamos National Lab., 1996.

(10) (a) Hemmatifar, A.; Ozbek, N.; Halliday, C.; Hatton, T. A. Electrochemical Selective Recovery of Heavy Metal Vanadium Oxyanion from Continuously Flowing Aqueous Streams. *ChemSusChem* **2020**, *13* (15), 3865−3874. (b) Ren, Y.; Mao, X.; Hatton, T. A. An Asymmetric Electrochemical System with Complementary Tunability in Hydrophobicity for Selective Separations of Organics. *ACS Cent. Sci.* **2019**, *5* (8), 1396−1406. (c) Su, X.; Kushima, A.; Halliday, C.; Zhou, J.; Li, J.; Hatton, T. A. Electrochemically-mediated selective capture of heavy metal chromium and arsenic oxyanions from water. *Nat. Commun.* **2018**, *9*, 4701. (d) Tan, K.-J.; Su, X.; Hatton, T. A. An Asymmetric Iron-Based Redox-Active System for Electrochemical Separation of Ions in Aqueous Media. *Adv. Funct. Mater.* **2020**, *30* (15), 1910363.

(11) Kim, K.; Cotty, S.; Elbert, J.; Chen, R.; Hou, C. H.; Su, X. Asymmetric Redox-Polymer Interfaces for Electrochemical Reactive Separations: Synergistic Capture and Conversion of Arsenic. *Adv. Mater.* **2020**, *32* (6), No. e1906877.

(12) Glidle, A.; Cooper, J.; Hillman, A. R.; Bailey, L.; Jackson, A.; Webster, J. R. Redox Controlled Partition and Spatial Distribution of Solvent and Salt in Electroactive Polyvinylferrocene Films. *Langmuir* **2003**, *19* (19), 7746−7753.

(13) Fleischmann, S.; Zhang, Y.; Wang, X.; Cummings, P. T.; Wu, J.; Simon, P.; Gogotsi, Y.; Presser, V.; Augustyn, V. Continuous transition from double-layer to Faradaic charge storage in confined electrolytes. *Nat. Energy* **2022**, *7*, 222−228.

(14) (a) Valincius, G.; Niaura, G.; Kazakeviciene, B.; Talaikyte, Z.; Kazemekaite, M.; Butkus, E.; Razumas, V. Anion effect on mediated electron transfer through ferrocene-terminated self-assembled monolayers. *Langmuir* **2004**, *20* (16), 6631−6638. (b) Nishiyama, K.; Ueda, A.; Tanoue, S.; Koga, T.; Taniguchi, I. Direct Observation of Perchlorate Incorporation Induced by Redox Reaction of Ferrocene Terminated Self-Assembled Monolayer Studied byin situFT-Surface Enhanced Raman Spectroscopy. *Chem. Lett.* **2000**, *29* (8), 930−931. (c) Rudnev, A. V.; Zhumaev, U.; Utsunomiya, T.; Fan, C.; Yokota, Y.; Fukui, K.-i.; Wandlowski, T. Ferrocene-terminated alkanethiol self-assembled monolayers: An electrochemical and in situ surface-enhanced infra-red absorption spectroscopy study. *Electrochim. Acta* **2013**, *107*, 33−44. (d) Robert Hillman, A.; Taylor, D. A.; Hamnett, A.; Higgins, S. J. Ellipsometric studies of ferrocene-containing copolymer films. *J. Electroanal. Chem. Interfacial Electrochem.* **1989**, *266* (2), 423−435. (e) Hillman, A. R.; Loveday, D. C.; Swann, M. J.; Eales, R. M.; Hamnett, A.; Higgins, S. J.; Bruckenstein, S.; Wilde, C. P. Charge transport in electroactive polymer films. *Faraday Discuss. Chem. Soc.* **1989**, *88*, 151−163. (f) Schlindwein, W. S.; Kavvada, A.; Linford, R. G.; Latham, R. J.; Günter Grossmann, J. Combined XAS/SAXS/Electrochemical studies on the conformation of poly (vinylferrocene) under redox conditions. *Ionics* **2002**, *8* (1−2), 85−91. (g) Balasubramanian, M.; Giacomini, M. T.; Lee, H. S.; McBreen, J.; Sukamto, J. H. X-Ray Absorption Studies of Poly(vinylferrocene) Polymers for Anion Separation. *J. Electrochem. Soc.* **2002**, *149* (9), D137. (h) Inzelt, G.; Horányi, G.; Chambers, J. Q. Radiotracer study of the sorption of counter- and co-ions in tetracyanoquinodimethane and poly(vinyl ferrocene) modified electrodes. *Electrochim. Acta* **1987**, *32* (5), 757−763. (i) Barbero, C.; Miras, M.; Calvo, E.; Kötz, R.; Haas, O. A probe beam deflection study of ion exchange at poly (vinylferrocene) films in aqueous and nonaqueous electrolytes. *Langmuir* **2002**, *18* (7), 2756−2764. (j) Fan, F. R. F.; Mirkin, M. V.; Bard, A. J. Polymer films on electrodes. 25. Effect of polymer resistance on the electrochemistry of poly (vinylferrocene): scanning electrochemical microscopic, chronoamperometric, and cyclic voltammetric studies. *J. Phys. Chem.* **1994**, *98* (5), 1475−1481. (k) Hunter, T. B.; Tyler, P. S.; Smyrl, W. H.; White, H. S. Impedance analysis of poly (vinylferrocene) films: the dependence of diffusional charge transport and exchange current density on polymer oxidation state. *J. Electrochem. Soc.* **1987**, *134* (9), 2198−2204. (l) Carlin, C. M.; Kepley, L. J.; Bard, A. J. Polymer films on electrodes: XVI. In situ ellipsometric measurements of polybipyrazine, polyaniline, and polyvinylferrocene films. *J. Electrochem. Soc.* **1985**, *132* (2), 353−359. (m) Leddy, J.; Bard, A. J. Polymer films on electrodes: Part XII. Chronoamperometric and rotating disk electrode determination of the mechanism of mass transport through poly (vinyl ferrocene) films. *J. Electroanal. Chem. Interfacial Electrochem.* **1983**, *153* (1−2), 223−242. (n) Peerce, P. J.; Bard, A. J. Polymer films on electrodes: Part III. Digital simulation model for cyclic voltammetry of electroactive polymer film and electrochemistry of poly (vinylferrocene) on platinum. *J. Electroanal. Chem. Interfacial Electrochem.* **1980**, *114* (1), 89−115. (o) Bandey, H. L.; Gonsalves, M.; Hillman, A. R.; Glidle, A.; Bruckenstein, S. Dynamic quartz crystal impedance measurements of polyvinylferrocene film deposition. *J. Electroanal. Chem.* **1996**, *410* (2), 219−227. (p) Pater, E. M.; Bruckenstein, S.; Robert Hillman, A. Film mass and volume changes accompanying redox-driven solvent and salt transfer during redox switching of polyvinylferrocene films. *J. Chem. Soc., Faraday Trans.* **1998**, *94* (8), 1097−1103. (q) Jureviciute, I.; Bruckenstein, S.; Hillman, A. R. Counter-ion specific effects on charge and solvent trapping in poly (vinylferrocene) films. *J. Electroanal. Chem.* **2000**, *488* (1), 73−81.

(15) Hillman, A. R.; Hughes, N. A.; Bruckenstein, S. Solvation phenomena in polyvinylferrocene films: effect of history and redox state. *J. Electrochem. Soc.* **1992**, *139* (1), 74−77.

(16) Glidle, A.; Hillman, A. R.; Ryder, K. S.; Smith, E. L.; Cooper, J.; Gadegaard, N.; Webster, J. R.; Dalgliesh, R.; Cubitt, R. Use of neutron reflectivity to measure the dynamics of solvation and structural changes in polyvinylferrocene films during electrochemically controlled redox cycling. *Langmuir* **2009**, *25* (7), 4093−4103.

(17) Hillman, A. R.; Loveday, D. C.; Bruckenstein, S. Thermodynamic changes in ion and solvent populations accompanying redox switching in polyvinylferrocene films. *J. Electroanal. Chem. Interfacial Electrochem.* **1989**, *274* (1−2), 157−166.

(18) Jureviciute, I.; Jackson, A.; Hillman, A. R.; Bruckenstein, S. Redox history effects accompanying the electrochemical cycling of poly(vinylferrocene). *J. Solid State Electrochem.* **2004**, *8* (6), 403−410.



https://doi.org/10.1021/jacsau.3c00705
*JACS Au* 2024, 4, 919−929

(19) (a) Tan, K. J.; Morikawa, S.; Hemmatifar, A.; Ozbek, N.; Liu, Y.; Hatton, T. A. Hydrophobicity Tuned Polymeric Redox Materials with Solution-Specific Electroactive Properties for Selective Electrochemical Metal Ion Recovery in Aqueous Environments. *ACS Appl. Mater. Interfaces* **2023**, *15* (37), 43859−43870. (b) Chen, R.; Wang, H.; Doucet, M.; Browning, J. F.; Su, X. Thermo-Electro-Responsive Redox-Copolymers for Amplified Solvation, Morphological Control, and Tunable Ion Interactions. *JACS Au* **2023**, *3*, 3333−3344.
(20) (a) Bard, A. J.; Faulkner, L. R.; White, H. S. *Electrochemical Methods: Fundamentals and Applications*; John Wiley & Sons, 2022. (b) Cheng, H.; Sun, Q.; Li, L.; Zou, Y.; Wang, Y.; Cai, T.; Zhao, F.; Liu, G.; Ma, Z.; Wahyudi, W.; et al. Emerging Era of Electrolyte Solvation Structure and Interfacial Model in Batteries. *ACS Energy Lett.* **2022**, *7* (1), 490−513.
(21) Shen, L.; Tesfaye, F.; Li, X.; Lindberg, D.; Taskinen, P. Review of rhenium extraction and recycling technologies from primary and secondary resources. *Miner. Eng.* **2021**, *161*, 106719.
(22) Virolainen, S.; Laatikainen, M.; Sainio, T. Ion exchange recovery of rhenium from industrially relevant sulfate solutions: Single column separations and modeling. *Hydrometallurgy* **2015**, *158*, 74−82.
(23) (a) Djamali, E.; Chen, K.; Cobble, J. W. Standard state thermodynamic properties of aqueous sodium perrhenate using high dilution calorimetry up to 598.15K. *J. Chem. Thermodyn.* **2009**, *41* (9), 1035−1041. (b) Banerjee, D.; Kim, D.; Schweiger, M. J.; Kruger, A. A.; Thallapally, P. K. Removal of TcO4(−) ions from solution: materials and future outlook. *Chem. Soc. Rev.* **2016**, *45* (10), 2724−2739.
(24) Marcus, Y. *Ions in Solution and Their Solvation*; John Wiley & Sons, 2015.
(25) (a) Wei, J.; Hoagland, D. A.; Zhang, G.; Su, Z. Effect of Divalent Counterions on Polyelectrolyte Multilayer Properties. *Macromolecules* **2016**, *49* (5), 1790−1797. (b) Inzelt, G. Role of polymeric properties in the electrochemical behaviour of redox polymer-modified electrodes. *Electrochim. Acta* **1989**, *34* (2), 83−91.
(26) Mao, X.; Rutledge, G. C.; Hatton, T. A. Polyvinylferrocene for noncovalent dispersion and redox-controlled precipitation of carbon nanotubes in nonaqueous media. *Langmuir* **2013**, *29* (31), 9626−9634.
(27) Johansson, A.; Kollman, P.; Rothenberg, S.; McKelvey, J. Hydrogen bonding ability of the amide group. *J. Am. Chem. Soc.* **1974**, *96* (12), 3794−3800.
(28) Elbert, J.; Gallei, M.; Rüttiger, C.; Brunsen, A.; Didzoleit, H.; Stühn, B.; Rehahn, M. Ferrocene Polymers for Switchable Surface Wettability. *Organometallics* **2013**, *32* (20), 5873−5878.
(29) Smiechowski, M.; Persson, I. Hydration of Oxometallate Ions in Aqueous Solution. *Inorg. Chem.* **2020**, *59* (12), 8231−8239.
(30) Baldaguez Medina, P.; Ardila Contreras, V.; Hartmann, F.; Schmitt, D.; Klimek, A.; Elbert, J.; Gallei, M.; Su, X. Investigating the Electrochemically Driven Capture and Release of Long-Chain PFAS by Redox Metallopolymer Sorbents. *ACS Appl. Mater. Interfaces* **2023**, *15* (18), 22112−22122.
(31) Kim, N.; Vijaya Sundar, J.; Elbert, J.; Seo, S. J.; Mironenko, A. V.; Su, X. Redox-responsive halogen bonding as a highly selective interaction for electrochemical separations. *Adv. Mater.* **2024**. under review.
(32) Baldwin, M. G.; Johnson, K. E. Free-radical polymerization of vinyl ferrocene. *J. Polym. Sci., Part A-1: Polym. Chem.* **1967**, *5* (8), 2091−2098.
(33) Sauerbrey, G. The use of quarts oscillators for weighing thin layers and for microweighing. *Z. Phys.* **1959**, *155*, 206−222.
(34) Vrugt, J. A.; ter Braak, C. J. F.; Diks, C. G. H.; Robinson, B. A.; Hyman, J. M.; Higdon, D. Accelerating Markov Chain Monte Carlo Simulation by Differential Evolution with Self-Adaptive Randomized Subspace Sampling. *Int. J. Nonlinear Sci. Numer. Simul.* **2009**, *10* (3), 273.
(35) Maranville, B. B.; Kienzle, P.; Sheridan, R.; Doucet, M.; Nelson, A.; Hoogerheide, D. P.; Book, A.; Balakrishnan, P. P.; Ghose, R.; Caruana, A. *reflectometry/refl1d: v0.8.16*; Zenodo, 2023.
(36) Su, X.; Kulik, H. J.; Jamison, T. F.; Hatton, T. A. Anion-Selective Redox Electrodes: Electrochemically Mediated Separation with Heterogeneous Organometallic Interfaces. *Adv. Funct. Mater.* **2016**, *26* (20), 3394−3404.
(37) Kuhne, T. D.; Iannuzzi, M.; Del Ben, M.; Rybkin, V. V.; Seewald, P.; Stein, F.; Laino, T.; Khaliullin, R. Z.; Schutt, O.; Schiffmann, F.; et al. CP2K: An electronic structure and molecular dynamics software package - Quickstep: Efficient and accurate electronic structure calculations. *J. Chem. Phys.* **2020**, *152* (19), 194103.
(38) (a) Perdew, J. P.; Burke, K.; Ernzerhof, M. Generalized gradient approximation made simple. *Phys. Rev. Lett.* **1996**, *77* (18), 3865−3868. (b) Grimme, S.; Antony, J.; Ehrlich, S.; Krieg, H. A consistent and accurate ab initio parametrization of density functional dispersion correction (DFT-D) for the 94 elements H-Pu. *J. Chem. Phys.* **2010**, *132* (15), 154104.
(39) Lippert, G.; Hutter, J.; Parrinello, M. A hybrid Gaussian and plane wave density functional scheme. *Mol. Phys.* **1997**, *92* (3), 477−487.
(40) VandeVondele, J.; Hutter, J. Gaussian basis sets for accurate calculations on molecular systems in gas and condensed phases. *J. Chem. Phys.* **2007**, *127* (11), 114105.
(41) Goedecker, S.; Teter, M.; Hutter, J. Separable dual-space Gaussian pseudopotentials. *Phys. Rev. B* **1996**, *54* (3), 1703−1710.
(42) Bengtsson, L. Dipole correction for surface supercell calculations. *Phys. Rev. B: Condens. Matter Mater. Phys.* **1999**, *59* (19), 12301−12304.
(43) Fabbrizzi, L. The ferrocenium/ferrocene couple: a versatile redox switch. *ChemTexts* **2020**, *6*, 22.
(44) Evans, D. J.; Holian, B. L. The nose-hoover thermostat. *J. Chem. Phys.* **1985**, *83* (8), 4069−4074.


https://doi.org/10.1021/jacsau.3c00705
*JACS Au* 2024, 4, 919−929